Engineering and Technology Journal
Journal homepage: https://etj.uotechnology.edu.iq

Effect of Adding MgO on Microstructure of Zirconia Toughened Alumina (ZTA) Composite for Medical Applications

Alaa S. Taeh*, Farhad M. Othman, Alaa A. Abdul-Hamead

Materials Engineering Dept., University of Technology-Iraq, Alsina'a street, 10066 Baghdad, Iraq.
*Corresponding author Email: mailto:alaataeh@uowasit.edu.iq

HIGHLIGHTS

- Synthesis of the ZTA composite using the sol-gel technique starting from salts.
- The sol-gel technique was used to create a ZTA + xMgO composite starting with salts.
- With an increase in MgO concentration, the grain size was reduced from 41.82 nm to 31.88 and 26.83 nm, respectively.
- The antibacterial activity of ZTA improved by adding xMgO.

ARTICLE INFO

Handling editor: **Basma I. Waisi**

Keywords:
ZTA composite; MgO nanoparticles; antibacterial activity; sol-gel method; biomaterials.

ABSTRACT

Zirconia toughened alumina (Biolox delta) is a new-generation ceramic with four times the strength of alumina alone, used in artificial joints. The composite ZTA, consisting of 82 wt. %Al_2O_3, 17 wt. % ZrO_2, 0.5 wt. % Cr_2O_3, and 0.5 wt. % SrO, was made using the sol-gel process, starting with salts. To investigate the effects of MgO on the ZTA microstructure, two concentrations (0.25 and 0.5 wt. %) of MgO were added to biolox during gelation to study the ZTA microstructure. Powders were sintered in the air for 2 hrs. at 1450 ºC. X-ray diffraction (XRD), scanning electron microscopy (SEM), and energy dispersive x-ray analysis (EDX) were used to characterize sintering powders. ZTA + xMgO structural characteristics differ from pure ZTA's. According to XRD calculations, grainsize decreased from 41.82 nm to 31.88 and 26.83 nm with increasing MgO concentration, but the specific surface area (SSA) increased from 40.63 to 54.79 m^2/gm while crystallization improved. SEM examination shows the composite has a homogeneous dispersion of shaped particles. The EDX test shows the composite's homogeneous element distribution. ZTA+ xMgO powders were more antibacterial than ZTA powders. MgO inhibits bacterial activity and grain formation in ZTA composite during sintering, which makes it a good choice for medical applications, mainly artificial joints.

1. Introduction

One of the major aims of the industry of modern materials technology is to produce new materials that will improve the quality of life and extend the productive years of human life. Ceramic materials, compared to metals and polymers, have a greater degree of biological compatibility with body tissues; consequently, there is substantial demand for ceramic materials in the area of medical treatment owing to this element of their qualities [1,2]. Monophasic oxide ceramics depending on corundum (α-Al_2O_3), as well as solid solutions with tetragonal modification t-ZrO_2 (TZP), is used in surgeries to treat a wide variety of conditions, such as spine deformities, orthotropic diseases, and dental restorations. The biological reaction to their presence is normally weak; they do not elicit negative immunological responses or cause the body to remove them as a foreign material[3,4].the based composite contents (with Al_2O_3 in the range of 60-95%vol.) Zirconia toughened alumina (ZTA) composites have been the topic of a large amount of study [5]. Ceram Tec Ag of Plochingen, Germany, began making ZTA accessible as a femoral head material in June of 2000.

The biolox delta brand was used for advertising and selling this material. Shortly after receiving FDA approval in 2003, ZTA started extensive use in THA. Approximately one million ceramtec ZTA femoral heads and over 700,000 inserts have been implanted in patients worldwide during the past decade [3]. The outstanding properties of biolox delta rely on complex reinforcing mechanisms. Therefore, it is necessary to assess if reinforcement is maintained throughout the lifetime of the artificial joint, which is anticipated to exceed more than 20 years. It is shown that the advantageous properties of this material are based on the reinforcing mechanisms which are activated due to the unique composition of this material.

The main constituents, especially alumina and zirconia, have unique features. Alumina is defined by its excellent hardness, resistance to corrosion, and bio-compatibility. The wear behavior of pure alumina components is excellent [6]. In vivo, ceramic wear debris has a lower inflammatory or granuloma formation response than metallic or polyethylene particles. Alumina for

http://doi.org/10.30684/etj.2022.134694.1245
Received 13 July 2022; Accepted 02 September 2022; Available online 07 October 2022

hip joints has previously been developed, with improved raw material quality, production, and quality control, resulting in a considerable decrease in fracture risk. But the average strength of alumina is only about 650 MPa (as measured by 4-point bending according to ISO 6474-1) [7].

Along with the main components, the material also has stabilizing elements. For example, the alumina matrix is mixed with chromium, which dissolves in the alumina matrix and makes the composite harder. Also, some yttrium is added to the composite. This yttrium dissolves in the zirconia and helps stabilize the tetragonal phase [8].

The creation of the ceramic composite powder may be achieved in various ways, including mechanical mixing, the sol-gel method, hydrothermal oxidation, and so on. Then, the powder is sintered [8, 9]. Nevertheless, due to the agglomeration of nanoparticles and abnormal grain growth during the subsequent sintering process, it is still very difficult to prepare ZTA with ultra-fine and uniform nanostructures. So, excessive grain growth must be avoided during high-temperature sintering. This is because large grains in a matrix of very fine-grained crystals lead to stress concentration, which increases the chance that cracks will start when the material is loaded and unloaded repeatedly and lowers the properties of the material [10]. As mentioned above, different oxides like (calcium fluoride CaF_2 [11], magnesium oxide MgO [12], lanthanum oxide La_2O_3 [13], barium fluoride BaF_2 [14], tungsten supplied WS_2 [15]) are used to inhibit grain growth and refines microstructure. Still, they have a different effect on other material properties. MgO is an important inorganic oxide widely used in various fields. Numerous investigations have shown magnesium oxide nanoparticles have potent antibacterial actions [16].

The mineral magnesium oxide (MgO) has been extensively utilized as a bone implant material for many years and has shown exceptional biocompatibility and superior mechanical properties [17]. MgO is often utilized as a sintering aid for ceramic materials because it becomes a liquid at high temperatures at the grain boundary, lowering the sintering temperature of the ceramics. MgO may also be used to control grain development [18].in the field of orthopedics, biomaterials that have been medically implanted are prone to bacterial infection, which may result in implant failure and other consequences, such as wide-spread infection [1]. To solve these problems, the researchers studied magnesium oxide (MgO) nanoparticles as advanced materials that might promote orthopedic tissue regeneration while decreasing the risk of bacterial infection [19]. MgO nanoparticles have been found to stimulate bone tissue formation and have been extensively employed as bone tissue engineering materials in recent years. As a result, the adhesion and proliferation of osteoblasts and fibroblasts were shown to be increased in the presence of MgO nanoparticles [20]. On the other hand, MgO nanocomposites had excellent bactericidal effectiveness, killing virtually all of the bacteria seeded onto them. Furthermore, by altering the size and concentration of nanoparticles inside the composite, the mechanical characteristics of the material might be modified to match those of bone or ligament tissues [6]. Homogenous distribution of ZrO_2 is important to consider when improving the micro-crack nucleation-induced toughening of a ceramic matrix. The homogeneity of zirconia particles throughout the alumina matrix may be controlled using homogeneous powder manufacturing techniques [21,22]. A variety of powder processing procedures have been investigated. First, to generate a homogeneous powder combination. Precipitation and sol–gel synthesis are two of the most simple and extensively utilized chemical synthesis processes for creating zirconia doped nanoparticles. They have both been employed effectively in commercial settings [5,16].

Manufacturing ZrO_2 dispersed Al_2O_3 precursor powders from multiphase hydrogel is a difficult process that depends on the arrangement of the Al and Zr hydroxide and the polymerization process. Aluminum oxide, hydroxide chemistry, and polymerization are regulated by acid-base properties [23, 17].

This paper aimed to strive to develop a ZTA composite microstructure by an effective technique of adding different concentrations of MgO because, by changing the size and concentration of nanoparticles inside the composite, the mechanical properties of the material could be changed to match those of artificial joints, which would reduce the risk of fractures by a large amount. In this work, ZTA/xMgO composite synthesis by the sol-gel method was unveiled, which eloquently enhanced the microstructure properties and investigated the effects of adding mgo on the zta microstructure biological properties by XRD, FE-SEM, and EDX is presented.

2. Experimental Part

2.1 Preparation of ZTA Powder

Sol-gel technology was utilized to synthesize ZTA from alumina, zirconia, yttria, strontium, and chromium precursor materials. The raw materials used to fabricate the ceramic composites are listed in Table 1 with their properties.

Table 1: The raw materials used to fabricate the ceramic composites

Raw Materials	Formulation	Purity %	Molecular weight (g/mol)	Physical state	Origin (manufacture)
Aluminum Chloride Hexahydrate	$AlCL_3.6H_2O$	97	241.43	Solid	CDH, India

Table 1: Continued

Zirconium (IV) Chloride	$ZrOCl_2.8H_2O$	99	322.25	Solid	Merck Darmstadt, Germany
Yttrium(III) Nitrate Hexahydrate	$Y(NO_3)_3.6H_2O$	99.8	383 .01	Solid	Sigma – Aldrich, United States
Chromium(III) Chloride Hexahydrate	$CrCl_3.6H_2O$	98	266.45	Solid	Spectrum, United States
Strontium Dicloride Hexahydrate	$SrCl_2.6H_2O$	98	281.21	Sold	Spectrum, United States
Magnesium Sulfate Heptahydrate	$MgSO_4.7H_2O$	99	246.48	Solid	Alfa Aesar, England
Ammonia	NH_3	98	40	Liquid	Alph Chemika, India

In distilled water, $AlCl_3$. $6H_2O$ was hydrolyzed. Separately, partly stabilized zirconia was made by $Y(NO_3)_3.4H_2O$ to $ZrOCl_2.8H_2O$ and then hydrolyzed the mixture Figure 1.

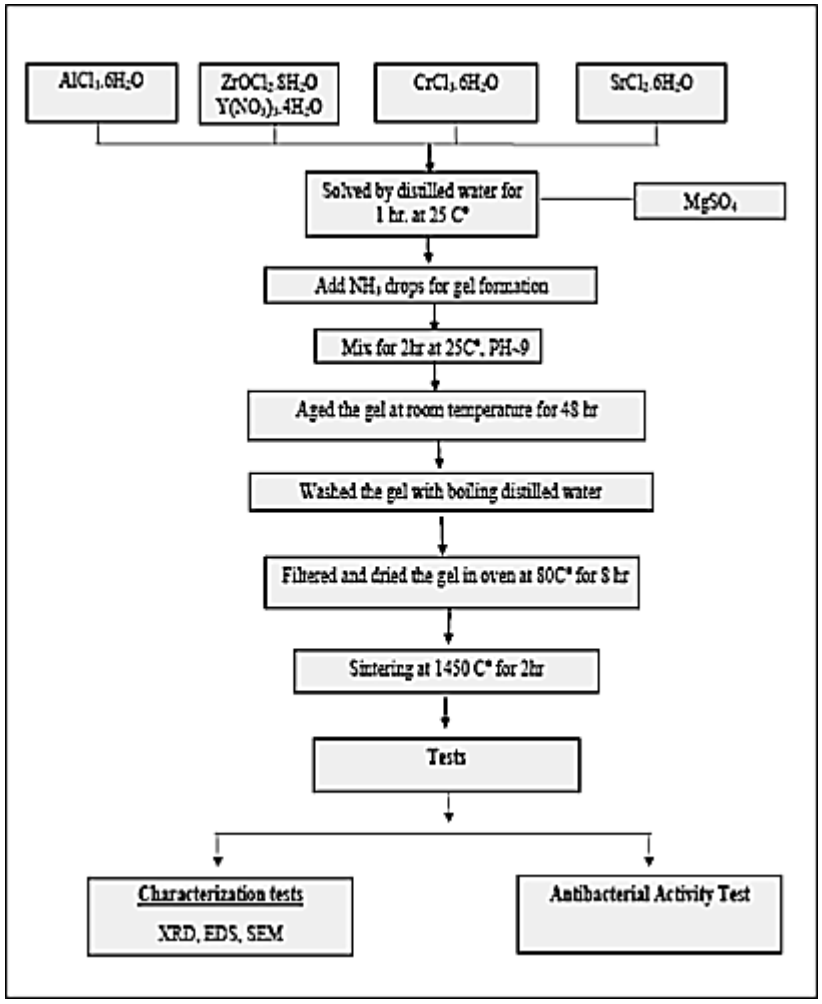

Figure 1: steps of fabrication of ZTA powders

The mixture was carefully stirred at 25 ºC. $CrCl_3.6H_2O$ and SrCl2·6H2O were hydrolyzed in distilled water (Figure 2a.Strontium and chromium precursors were added to the dissolved zirconium and aluminum mixtures. The mixture was mixed quite well for 2hrs. Then, subjected to an ultrasonic generator device at 30°C for 1hr. The mixed hydrogel was made by dropping a 1:1 NH_3 hydroxide solution into an aqueous solution of Al and Zr salt that was constantly agitated at 25 ° C. This was done again and again until the necessary uniformity was achieved. The viscosity of the batch slowly increased, and by the time it reached pH ~9, it had solidified into an intractable gel. Simultaneously, MgSO4 was dissolved separately in distilled

water at 25°C for 2hrs using a magnetic stirrer, then placed in an ultrasonic generator device at 30 °C for 1hr. The solution was kept stagnant for 3 hrs. to settle the particulate matter, then mixed with ZTA gel while stirring for 1 hr. Figure 2b.After that, the gels were allowed to age at room temperature for another 48 hrs. Then, the gel of each composition was filtered after being washed many times with distilled water and brought to a boil to remove any ions that included chloride or nitrate. The filter cake was baked in the oven at 80 ° C for 8 hrs. to dry it out. Using a muffle furnace (Carbolite, UK), the dry gels were calcined in the air at 1450 ° C for 2 hrs. The sintering powders were milled using mortar and pestle; the composition preparation steps are listed in Figure 2c.

(a)

(b)

(c)

Figure 2: steps of fabrication of ZTA a) salts dissolved in distilled water, b) mixing, adding hydroxide and forming a gel, c) filtering, drying, and forming powders

2.2 Experimental Tests

2.2.1 X-ray diffraction (XRD)

For phase analysis, an X-ray diffraction study of calcined powders was carried out by utilizing the X-ray diffraction (XRD) machine type (Philips PW1730); X-ray was created using Copper (Cu-Kα) radiation at 40 kV voltage, 30 mA current, and λ = 1.5406 Å wavelength.

The average grain size (D) for the synthesized powder was determined in nanometers from X-ray line broadening using Scherrer's Equation, as follows [24]:

$$D = \frac{0.94\,\lambda}{[\Delta_{2\theta}\, cos\theta]} \quad (1)$$

where: D: crystallite size (nm) λ: x-ray wavelength (1.54056 A°).$\Delta_{2\theta}$: FWHM; full width at half maximum (radian).θ: Bragg diffraction angle of the XRD peak (degree).

The crystal lattice constants for orthorhombic alumina, tetragonal zirconia, tetragonal $SrAl_{12}$-$Cr_xO_{19,}$ hexagonal Al_2O_4Sr, and cubic MgO nanoparticles, respectively, are shown below [25]:

$$\frac{1}{d_{hkl}^2} = \frac{h^2}{a^2} + \frac{k^2}{b^2} + \frac{l^2}{c^2} \quad (2)$$

$$\frac{1}{d_{hkl}^2} = \frac{h^2+k^2}{a^2} + \frac{l^2}{c^2} \quad (3)$$

$$\frac{1}{d_{hkl}^2} = \frac{4}{3}\left(\frac{h^2+hk+k^2}{a^2}\right) + \frac{l^2}{c^2} \quad (4)$$

$$\frac{1}{d_{hkl}^2} = \frac{(h^2+k^2+l^2)}{a^2} \quad (5)$$

where: *h, k*, and *l:* are Miller Coefficients*a, b*, and *c:* are the Lattice Constants

The number of defects present in the crystal may be measured by the dislocation density (δ) measure. An excellent level of crystallization was shown by the low value of the dislocation density. The dislocation density was calculated according to the following formula [26]:

$$\delta = \frac{1}{D_{av}^2} \quad (6)$$

Because of the nanoparticles' enormous surface-to-volume ratio and the accompanying reduction in crystallite size, the surface states will play an important role in the overall operation of the particles. One may determine the exact surface area by [24]:

$$S = \frac{6*10^3}{D_P\rho} \quad (7)$$

where:S: is the specific surface area. D_p: is the particle size.ρ: is the density of the material.

2.2.2 Field emission scanning electron microscope and energy dispersive X-Ray

Field Emission Scanning Electron Microscope imaging (FE-SEM type MiraIII – Tescan/ Czech) has been conducted with different magnifications for all powders (before and after adding) to examine the microstructure of powders.

The microstructure of powders was examined using a Scanning Electron Microscope (SEM) with Energy Dispersive X-Ray Spectroscopy (EDX, type Bruker–Germany), integrated with an Energy Dispersion Spectroscopy (EDS) apparatus to analyze the product powders.

2.2.3 Antibacterial activity test

The biological tests of powders were examined using the antibacterial activity test, which occurred at 37 ºC using two types of bacteria: gram-negative (E. coli) and gram-positive (Staphylococcus) according to ASTM E3031-20.

3. Results and Discussion

3.1 X-Ray Diffraction

The X-ray diffraction patterns were determined for nanocomposite powders of ZTA (biolox) with different percentages of additions after calcination at 1450°C for 2 hrs. These Figures were analyzed using a "match" software program.

The XRD pattern of the ZTA (biolox) after sintering is shown in Figure 3a. It has been shown that at 1450°C, powders have sharp peaks. This means that the crystallization was obtained at a high temperature at a suitable time. Furthermore, all the patterns' diffraction peaks match the standards of Entry Cod in the "match" software program for α-Al_2O_3, t-ZrO_2, $SrAl_{12}$-Cr_xO_{19}, Al_2O_4Sr, and small amounts of m-ZrO_2 (this phase appears due to cooling time after sintering), as shown in the Figure.

Using Scherrer's method mentioned in equation 1, the average crystallite size was attained at 41.82 nm for the ZTA complex, while the values for Al_2O_3, $ZrO_{2,}$ and alumina plate nanoparticles are illustrated in Table 2.

The lattice constants of crystal (a, b, c) were computed to prepare orthorhombic Al_2O_3, tetragonal zirconia, tetragonal $SrAl_{12}$-$Cr_xO_{19,}$ and hexagonal Al_2O_4Sr nanoparticles by using the relationships 2, 3, and 4, respectively [19]. It was discovered that the lattice parameter values are compatible with the values in the international card numbers, which are shown in Table 2 (96-100-0443, 96-152-1477, 96-810-3788, and 96-155-0866 for Orthorhombic alumina, Tetragonal zirconia, Tetragonal $SrAl_{12}$-Cr_xO_{19}, and Hexagonal Al_2O_4Sr nanoparticles, respectively).

The dislocation density (δ) is important for measuring the number of defects in the crystal. Therefore, the density of dislocations was calculated according to equation 6. The obtained value was ($5.718^{x}10^{-4}$ nm^{-2}), which was very small and confirmed the good crystallization of ZTA nanoparticles.

The surface states will play an important role in the nanoparticles because their surface-to-volume ratio is very high, and their crystallite size is getting smaller. Specific surface area, or SSA, is the area divided by the unit of mass (m^2/g). It is a very important property of nanomaterials and shows how good they are. It also tells us about the events that happen on the surface. Equation 7 was used, and the results demonstrated that the SSA value for ZTA was 40.63 m^2/g, indicating that the powder has a small particle size.

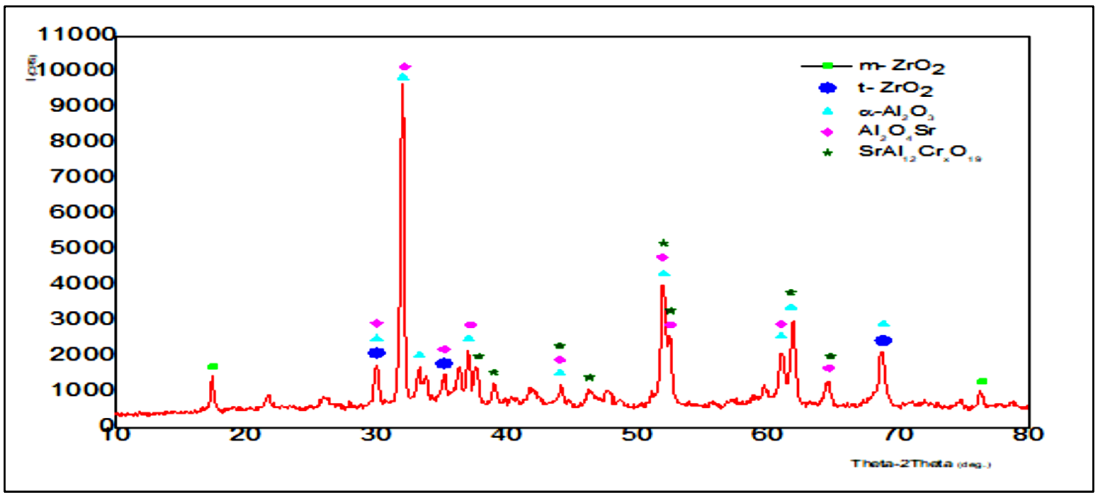

(a)

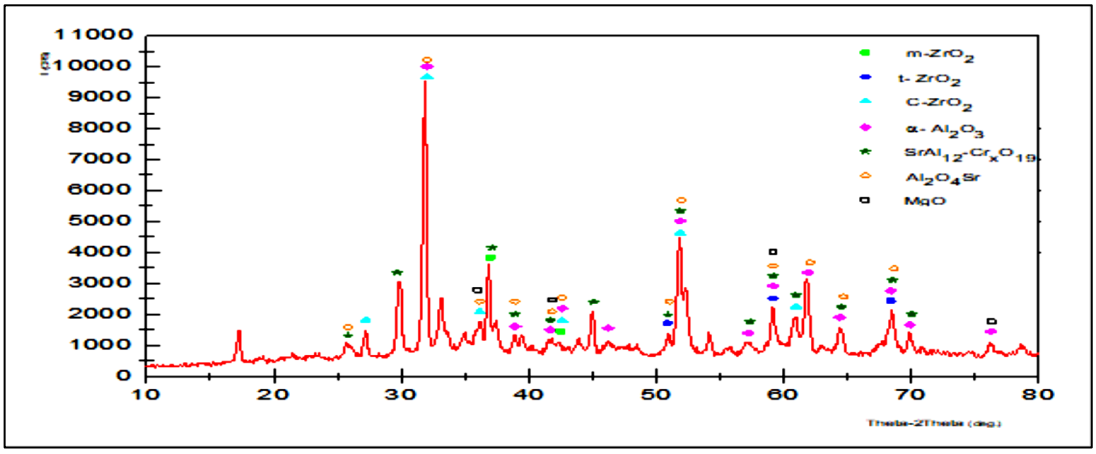

(b)

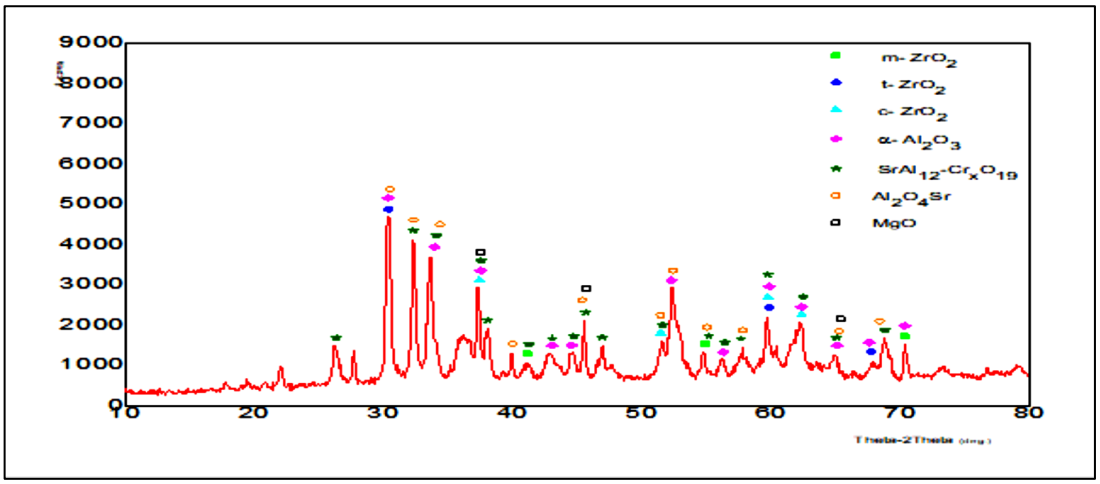

(c)

Figure 3: X-ray diffraction patterns for sintering a) ZTA (BIOLOX) b) ZTA + 0.25wt.% MgO c) ZTA + 0.5 wt.% MgO Powders

Table 2: Structural parameters of the ZTA nanoparticles

Sample	Average Crystallite Size(D)(nm)	Lattice Parameter Å	Dislocation Density ($\delta \times 10^{-4}$) (nm^{-2})	Specific Surface Area SSA(m^2/g)
ZTA Composite	41.82	---	5.7178	40.63
Al_2O_3	41.82	a=4.8546 b=8.3311 c=8.8841	5.7178	38.28
$YZrO_2$	29.26	a=b=3.6025 c=5.2942	11.6802	34.51
$SrAl_{12}$-Cr_xO_{19}	35.87	a=b=14.0782 c=9.3639	7.7721	51.66
Al_2O_4Sr	45.13	a=b=8.9406 c=8.4629	4.9099	38.06

The XRD patterns of the ZTA + xMgO composite powders (x = 0.25 and 0.5) are shown in Figures 3 (b and c). The X-ray diffraction patterns after sintering gave sharp peaks for powders. This means that the crystallization was obtained at a high temperature at a suitable time. All the diffraction peaks in the patterns match with the standards peaks of Entry Cod in a "match" software program for α-Al_2O_3, t-ZrO_2, $SrAl_{12}$-Cr_xO_{19}, Al_2O_4Sr, MgO, and small amounts of m-ZrO_2 (this phase appears due to cooling time after sintering) as shown in the Figures.

Also, small amounts of cubic ZrO_2 (matches Entry Cod 96-901-6444) appeared; due to sintering at high temperatures, the phase transformation for c-ZrO_2 was detected but not completely. That was because there were impurities or the temperature during sintering was not high enough [27].

Using Scherrer's method mentioned in Equation 1, the average crystallite size was attained for the ZTA composite after adding xMgO. The values for ZTA, Al_2O_3, ZrO_2, MgO, and alumina plate nanoparticles are illustrated in Tables 3 and 4. These values are smaller than the average crystallite sizes listed in Table 2 due to the pinning effect of MgO.

The crystal lattice constants (a, b, and c) were calculated, and their values are illustrated in Tables 3 and 4 for the prepared orthorhombic alumina, tetragonal zirconia, tetragonal $SrAl_{12}$-Cr_xO_{19}, hexagonal Al_2O_4Sr, and cubic MgO nanoparticles, which were calculated by using the relationships 2, 3, 4, and 5, respectively. The crystal lattice constants for all phases in ZTA+ xMgO are illustrated in the tables above. In addition, it was observed that the lattice constants' values match those in the international card numbers 96-100-0443, 96-152-1475, 96-810-3788, 96-155-0866, and 96-900-6765 for Orthorhombic alumina, Tetragonal zirconia, Tetragonal $SrAl_{12}$-Cr_xO_{19}, Hexagonal Al_2O_4Sr, and cubic MgO nanoparticles, respectively.

The Dislocation Density (δ) and Specific Surface Area (SSA) were calculated according to Equations 6 and 7, respectively. The values obtained are illustrated in Tables 3 and 4. The increase in dislocation density leads to the occurrence of substructures, encouraging the formation of small grain sizes. Also, the increase in the specific surface area (opposite SSA decrease) indicates the formation of small grain sizes.

Table 3: Structural parameters of the ZTA + 0.25% MgO nanoparticles

Sample	Average Crystallite Size (D) (nm)	Lattice Parameter Å	Dislocation Density ($\delta \times 10 -4$) ($nm -2$)	Specific Surface Area SSA(m2/g)
ZTA Composite	31.88	---	9.8393	48.40
Al_2O_3	33.997	a=4.8727 b=7.4733 c=9.0783	8.6521	47.09
$YZrO_2$	31.14	a=b=3.5879 c=5.2050	10.3125	32.02
$SrAl_{12}$-Cr_xO_{19}	31.88	a=b=13.3596 c=9.9069	9.8393	58.12
Al_2O_4Sr	31.88	a=b=8.8345 c=8.2497	9.8393	53.88
MgO	35.66	a= 4.3061	7.8639	50.88

Table 4: Structural parameters of the ZTA + 0.5% MgO nanoparticles

Sample	Average Crystallite Size (D) (nm)	Lattice Parameter Å	Dislocation Density (δ × 10 −4) (nm −2)	Specific Surface Area SSA(m2/g)
ZTA Composite	26.83	---	13.8918	54.79
Al_2O_3	28.94	a=4.7167 b=8.4189 c=8.7036	11.9340	55.32
$YZrO_2$	27.13	a=b=3.5912 c=5.1579	13.5863	36.75
$SrAl_{12}$-Cr_xO_{19}	31.42	a=b=13.5286 c=9.1967	10.1295	58.98
Al_2O_4Sr	26.83	a=b=9.0039 c=8.1044	13.8918	64.02
MgO	25.84	a=4.0980	14.9767	58.86

3.2 Field Emission Scanning Electron Microscopy (FE-SEM)

Field Emission Scanning Electron Microscopy imaging has been conducted with different magnifications for all powders (before and after adding) to observe their morphology and visually verify the success of crystallizations. In addition, the grain sizes of both fine and coarse grains were measured.

The FE-SEM images of ZTA nanocomposite powders sintered at 1450°C for 2 hrs. at various magnifications are shown in Figure 4a. It can be observed from these images that crystalline structures may be found in a wide range of sizes and shapes, including elongated, spherical, and semi-spherical forms. The Figures also showed the presence of clusters that included a large number of nanoparticles, which indicates that they were made when the smaller particles fused together during the precipitation or sintering process. The changes in the shape of the particles and the development of clusters are caused by the magnetic properties of the nanoparticles, which affect the morphology and size of the particles [26].

The FE-SEM images with different magnifications of nanocomposite powders for ZTA+ (0.25 and 0.5%) MgO powders after sintering at 1450°C for 2 hrs. are shown in Figures 4b and c. The FE-SEM images show that the crystalline structures may be found in many sizes and shapes, including elongated, spherical, and semi-spherical forms but also in small sizes. The images also showed clusters with a lot of nanoparticles, which means they were made when the smaller particles fused together during the precipitation or sintering process or because the nanoparticles had magnetic properties

The FE-SEM images for pure ZTA and ZTA+ xMgO show that the structure of composites is becoming more crystalline, and the grain size is becoming smaller when the concentration of MgO increases. There are also more round particles in the morphology than in pure ZTA.

The pinning effect of MgO was tied to the decrease in the observed ZTA particle size. The MgO inhabited the grain growth of the ZTA. This process may be characterized by the following: (i) less grain boundary mobility; (ii) more pore mobility as surface-promoting lattice and boundary diffusions increase; and (iv) less grain boundary anisotropy and grain surface energy [28].

3.3 Energy Dispersive X-Ray Spectroscopy (EDS)

SEM and EDX images were used to conduct surface analysis of the powder following calcination at 1450 ºC for 2 hrs. This was conducted to determine elements' distribution throughout the structure.

The results of EDX composition analysis of the prepared ZTA (Biolox) nanopowder composite are shown in Figure 5. The results of surface scanning show a homogenous distribution of elements in the structure. This suggests that the preparation technique used in this study is efficient for preparing nanocomposite powders. It is clear from the image that alumina covers practically the whole surface of the samples. The results of surface scanning for aluminum, zirconium, and oxygen show that those elements are present more in the structure of the sintered sample. The results also show that the surfaces they occupy are interloping. This overlap is caused by the fact that Cr, Sr, and Y are spread out in the structure. In the Figure, some peaks can be seen for other elements. They might be for other orbitals of Al, Zr, Sr, Cr, Y, or oxygen; otherwise, for impurities that are too small.

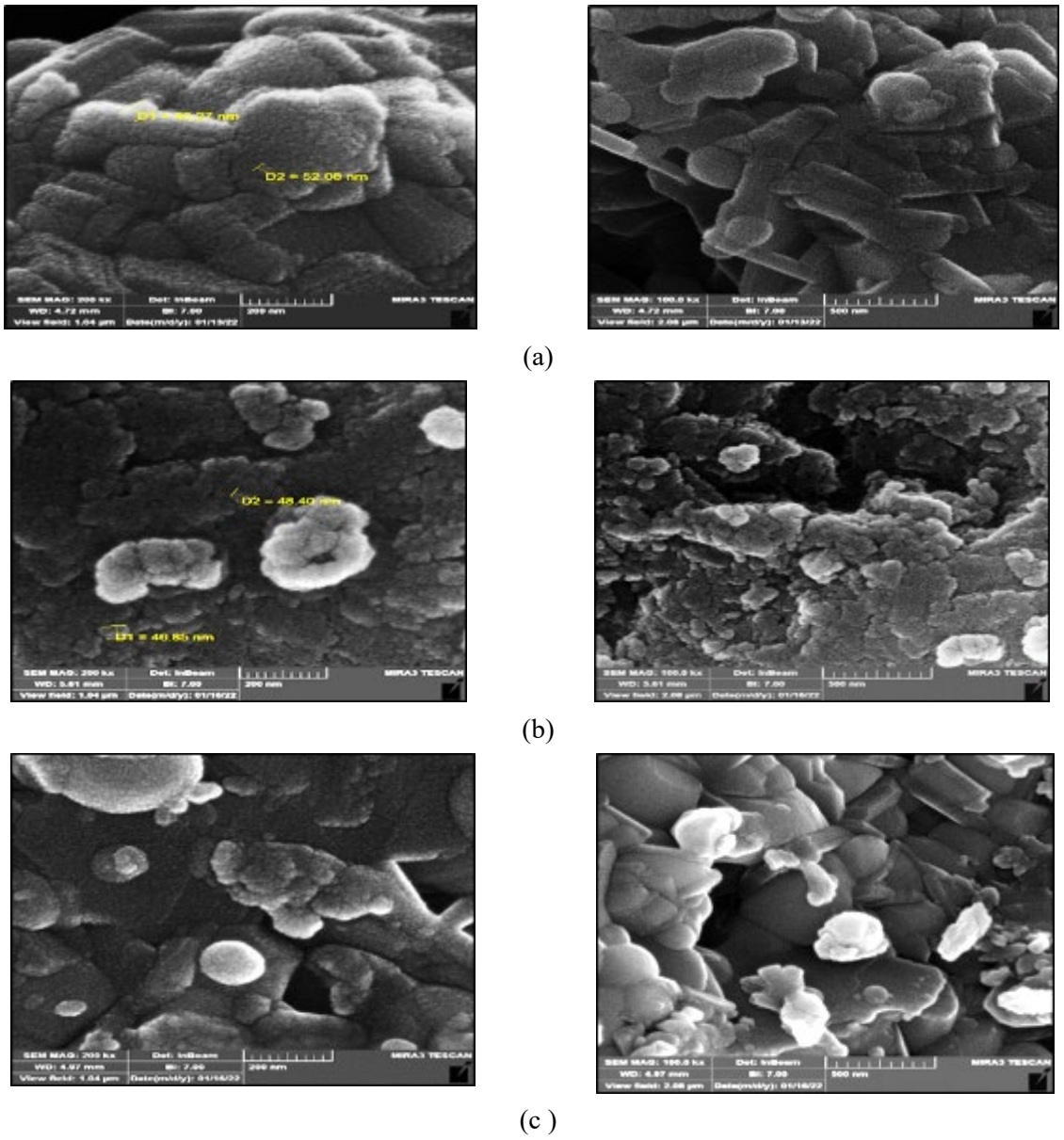

Figure 4: FE-SEM images with different magnifications for sintering a) ZTA (BIOLOX) b) ZTA + 0.25wt.% MgO c) ZTA + 0.5 wt.% MgO powders

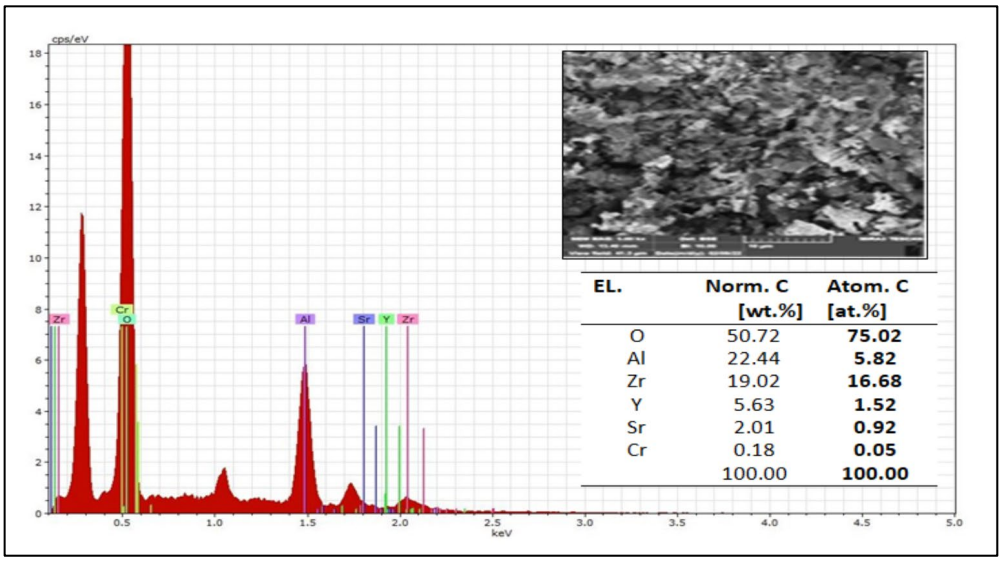

Figure 5: EDX for the sintered ZTA powder

The results of the EDX composition analysis of the prepared ZTA + xMgO nanopowder composite are shown in Figures 6 and 7. The findings of the surface scanning indicate that the components are distributed consistently throughout the structure; hence, this strengthens the argument that the production method used in this work is effective in manufacturing nanocomposite powders. It is clear from the Figure that alumina covers practically the whole surface of the samples. The results of surface scanning for aluminum, zirconium and oxygen show that those elements are present more in the structure of the sintered sample, and the results also show that the surfaces they occupy are inter-lapping, which corresponds to the presence of Cr, Sr, Y, and Mg dispersed throughout the structure. The Figures also demonstrate some peaks for other elements that might associate with other orbitals of Al, Zr, Sr, Cr, Y, or oxygen; otherwise, for impurities that are too small.

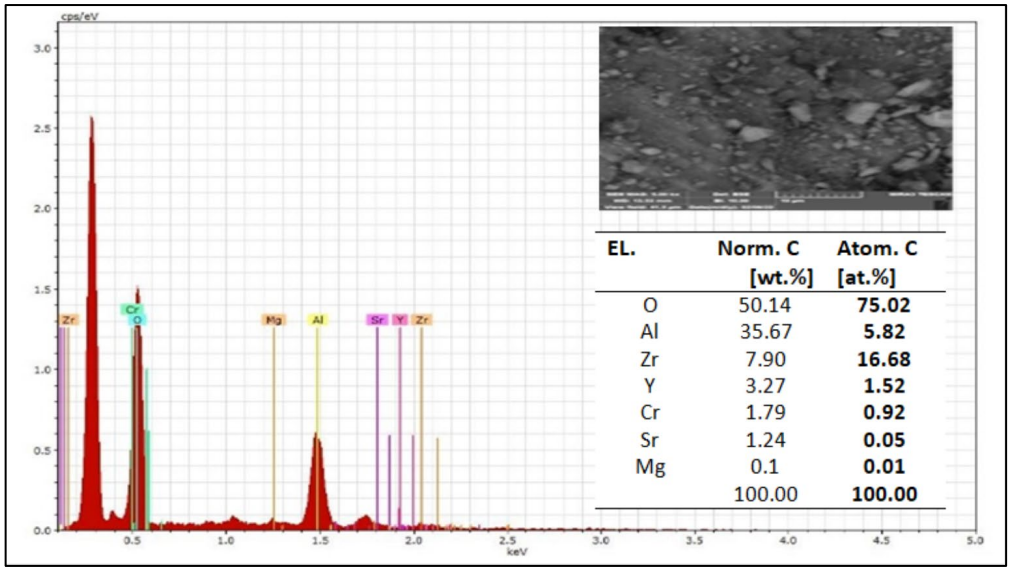

Figure 6: EDX for the sintering ZTA + 0.25%MgO powder

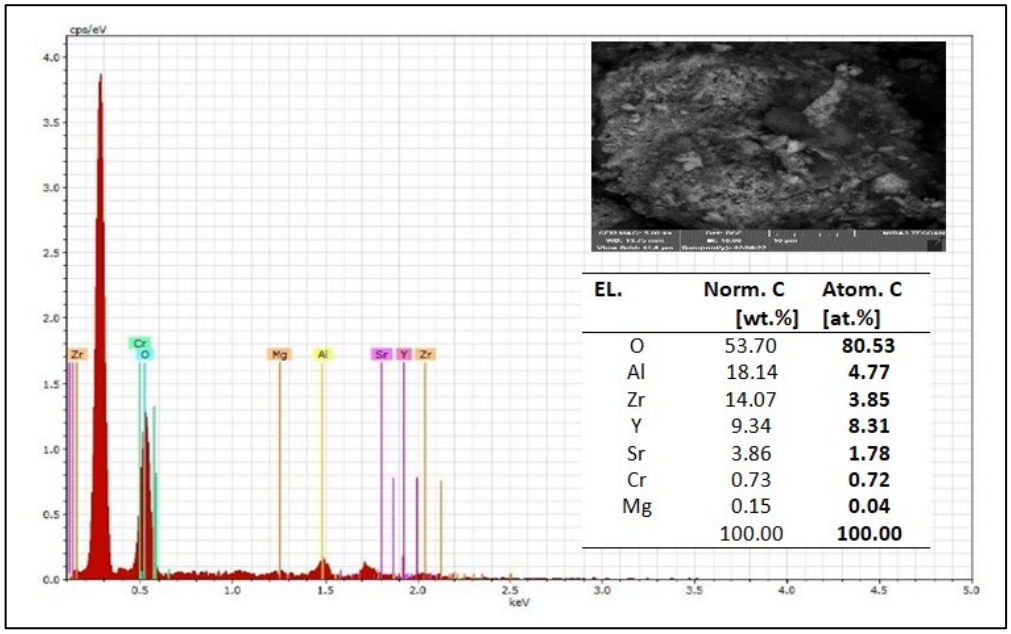

Figure 7: EDX for the sintering ZTA + 0.5%MgO powder

3.4 Antibacterial Activity Test

There is a great interest in generating antibacterial films because of their superior biomedical relevance. Even though many bioceramics have been used as surgical tools, they often cause bone irritation because they leach harmful chemicals into the body. The antibacterial activity of powders was determined by the disc diffusion method for E. coli and Staphylococcus, as shown in Table 5 and Figure 8. The antibacterial study results illustrate the potential ability of ZTA+ xMgO against microorganisms as a novel method for designing artificial joints that can be utilized for various therapeutic applications (bone replacement). The available xMgO additives were tested for antimicrobial assay and the synthesized nano ZTA to prove the influence of concentrations on antibacterial activity. Similar observations were shown in previous studies that demonstrated the effect of concentration on antibacterial activity [29]. The results from Figure 8b noted that the antibacterial activity of ZTA + xMgO powders had better properties than ZTA powders' antimicrobial agents Figure 8a, i.e., the highest concentrations of

MgO were inhibitory against bacteria. In addition, they had a higher affinity for interaction, which helped them work better with more bacterial and yeast cells and strengthened their antimicrobial effects.

The improved ZTA antibacterial activity is due to a decrease in ZTA particle size resulting from the MgO addition; i.e., smaller particles are inhibitory against bacteria, and larger particles exhibit decreased inhibitory activity. However, the antibacterial response mechanism of MgO is still not detected. There were some proposed mechanisms such as reactive oxygen species (ROS) diffusion such as superoxide anion (O^{2-}), the synergy of MgO nanoparticles against bacterial cells, following consumption of the pathogenic bacteria, and an alkaline attraction was introduced to explain the antimicrobial action mechanism. The MgO nanoparticles definitely changed the shape and layer structure of their cells. They also changed the permeability of bacterial membranes and caused oxidative pressure and gene responses inside bacterial cells by making H_2O_2 [22].

Table 5: Antibacterial activity of powders on pathogenic bacteria

Samples	E.coli (mm)	Staphylococcus (mm)
ZTA	10	12
ZTA + 0.25 MgO	11	11
ZTA + 0.5 MgO	12	11

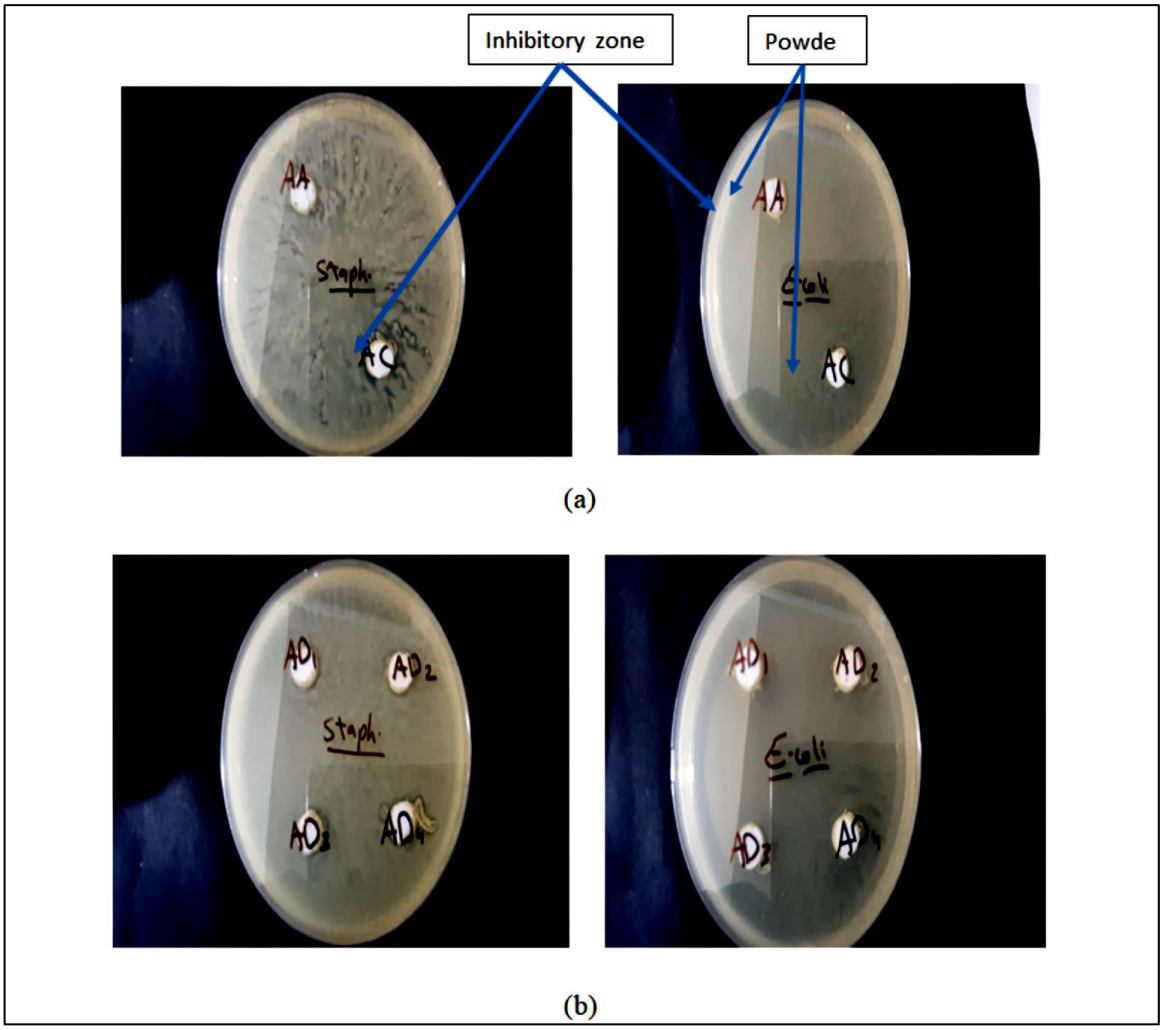

Figure 8: Inhibitory zone against pathogenic bacteria E. coli and Staphylococcus for a) ZTA samples b) ZTA + x MgO samples

4. Conclusions

The following significant findings may be taken from the current research:

1) Sol-gel technique is efficient for synthesizing nanocomposite powders (~26.83 nm), especially when wet mixing is used for starting materials.
2) With the addition of MgO, the microstructure characteristics of composite samples were significantly improved compared to those without MgO. In addition, compared to ZTA samples, the sintered composite

with additives may have facilitated greater crystallization in the elements, resulting in improved material characteristics.

3) According to XRD analysis, ZrO_2 transformation toughening decreased the monoclinic phase and enhanced the tetragonal phases, which resulted in better composite samples' mechanical characteristics. However, the sintering temperature at 1450 ºC is sufficient for alumina phase transformation to obtain α-phase, which is good for medical applications.
4) The EDX examination showed that the elements Al, Zr, Sr, Cr, Mg, and O were spread evenly, which is why we may anticipate an improvement in the characteristics of the composite samples that have been created.
5) The antibacterial activity of ZTA was enhanced when adding MgO and became better when the concentrations of MgO were increased because MgO acts as an inhibitory against bacteria.

Author contribution

All authors contributed equally to this work.

Funding

This research received no specific grant from any funding agency in the public, commercial, or not-for-profit sectors.

Data availability statement

The data that support the findings of this study are available on request from the corresponding author.

Conflicts of interest

The authors declare that there is no conflict of interest.

References

[1] B. S. Bal, J. P. Garino, M. D. Ries, Ceramics for Prosthetic Hip and Knee Joint Replacement, J. Am. Ceram. Soc., 90 (2007) 1965–1988. https://doi.org/10.1111/j.1551-2916.2007.01725.x

[2] S. R. Knight, R. Aujla, S. P. Biswas, 100 Years of Operative History Er Ci Us E on Er Al, Orthop. Rev., 3 (2011) 72–74. https://doi.org/10.4081/or.2011.16

[3] P.Palmero, L. Montanaro, H. Reveron, J.Chevalier, Surface Coating of Oxide Powders: A New Synthesis Method to Process Biomedical Grade Nano-Composites, Materials, 7 (2014) 5012–5037. https://doi.org/10.3390/ma7075012

[4] L. I. Podzorova et al., Materials For Ensuring Human Vital Activity Modified Composites Of Al_2O_3 – (Ce-Tzp) System As Materials For Medical Use, Inorg. Mater. Appl. Res., 7 (2016) 724–729. https://doi.org/10.1134/S207511331605021X

[5] D. Sarkar, D. Mohapatra, S. Ray, S. Bhattacharyya, S. Adak, N. Mitra, Synthesis and characterization of sol – gel derived ZrO_2 doped Al_2O_3 nanopowder, Ceram. Int., 33 (2007) 1275-1282. https://doi.org/10.1016/j.ceramint.2006.05.002

[6] D. J. Hickey, B. Ercan, S. Chung, T. J. Webster, L. Sun, B. Geilich, MgO nanocomposites as new antibacterial materials for orthopedic tissue engineering applications, 2014 40th Annual Northeast Bioengineering Conference (NEBEC), Boston, MA, USA, 2014, 1-2. https://doi.org/10.1109/NEBEC.2014.6972815

[7] C. Dauvergne , G. Fantozzi, Microstructural Investigation of the Aging Behavior of (3Y-TZP)–Al_2O_3 Composites ´, J. Am. Ceram. Soc., 88 (2005) 1273–1280. https://doi.org/10.1111/j.1551-2916.2005.00221.x

[8] V. Gopal , G. Manivasagam, Zirconia-alumina composite for orthopedic implant application, Applications of Nanocomposite Materials in Orthopedics, Elsevier, (2019) 201–219. https://doi.org/10.1016/B978-0-12-813740-6.00011-9

[9] J. G. Heinrich ,C. M. Gomes, Introduction to Ceramics Processing, J. Electrochem. Soc., 124 (1977) 152C.

[10] R. B. Helmann, The colour of medical-grade zirconia (Y-TZP), J. Mater. Sci. Mater. Med., 7 (1996) 559–565.

[11] K. K. Sadhu, S. Mazumder, P. Roy, S. Acharya, and B. Kumar, Synthesis and characterization of calcium fluoride added zirconia toughened alumina composite powder, IOP Conf. Ser.: Mater. Sci. Eng., 561, 2019, 012080 . https://doi.org/10.1088/1757-899X/561/1/012080

[12] A. Arab, Z. D. I. Sktani, Q. Zhou, Z. A. Ahmad, P. Chen, Effect of MgO addition on the mechanical and dynamic properties of zirconia toughened alumina (ZTA) ceramics, Materials, 12 (2019) 2440. https://doi.org/10.3390/ma12152440

[13] W. Yu, Y. Zheng, Y. Yu, X. Su, Combustion synthesis assisted water atomization-solid solution precipitation: A new guidance for nano-ZTA ceramics, J. Eur. Ceram. Soc., 39 (2019) 4313–4321. https://doi.org/10.1016/j.jeurceramsoc.2019.05.049

[14] S. Kim , S. Wohn, Wear and friction behavior of self-lubricating alumina – zirconia – fl uoride composites fabricated by the PECS technique, Ceram. Int., 40 (2014) 779–790. https://doi.org/10.1016/j.ceramint.2013.06.068

[15] M. Erkin Cura et al., Microstructure and tribological properties of pulsed electric current sintered alumina-zirconia nanocomposites with different solid lubricants, Ceram. Int., 39 (2013) 2093–2105. https://doi.org/10.1016/j.ceramint.2012.08.065

[16] Z. Tang , B. Lv, MgO nanoparticles as antibacterial agent: preparation and activity, Brazilian J. Chem. Eng., 31 (2014) 591–601. https://doi.org/10.1590/0104-6632.20140313s00002813

[17] A. Hussain et al., Formation of multifunctional ZrO_2–MgO-hBN nanocomposite for enhanced bone regeneration and E coli bacteria filtration applications, Ceram. Int., 46 (2020) 23006–23020. https://doi.org/10.1016/j.ceramint.2020.06.077

[18] Y. Zhang et al., Effect of MgO doping on properties of low zirconium content Ce-TZP/Al_2O_3 as a joint replacement material, Ceram. Int., 43 (2017) 2807–2814. https://doi.org/10.1016/j.ceramint.2016.11.122

[19] C. Y. Tan, A. Yaghoubi, S. Ramesh, S. Adzila, and J. Purbolaksono, Sintering and mechanical properties of MgO-doped nanocrystalline hydroxyapatite, Ceram. Int.,39 (2013) 8979–8983. https://doi.org/10.1016/j.ceramint.2013.04.098

[20] M. W. Akram et al., In vitro evaluation of the toxic effects of MgO nanostructure in Hela cell line, Sci. Rep., 8 (2017) 1–11. https://doi.org/10.1038/s41598-018-23105-y

[21] M. Catauro ,S. V. Ciprioti, Thermodynamics and Biophysics of Biomedical Nanosystems, Springer, 2019. https://doi.org/10.1007/978-981-13-0989-2

[22] N. Singh, R. Mazumder, P. Gupta, D. Kumar, Ceramic matrix composites: Processing techniques and recent advancements, J. Mater. Environ. Sci., 8 (2017) 1654–1660.

[23] D. Bokov et al., Nanomaterial by Sol-Gel Method: Synthesis and Application, Adv. Mater. Sci. Eng., 2021 (2021) 1-21. https://doi.org/10.1155/2021/5102014

[24] Parangusan, K. In uence of pH on Structural , Morphological , Optical , Photocatalytic , and Antibacterial Properties of Yttrium Oxide Nanoparticles via Co-Precipitation Method, Reserch Square, 2021. https://doi.org//10.21203/rs.3.rs-385905/v1 License.

[25] D. B. Miracle, F. Scheltens, P. R. Subramanian, Crystal structure determination of al$_2$ta, Philos. Mag. B Phys. Condens. Matter; Stat. Mech. Electron. Opt. Magn. Prop., 71 (1995) 941–953. https://doi.org/10.1080/01418639508243598

[26] A. A. Mohammed, Z. T. Khodair, and A. A. Khadom, Preparation and investigation of the structural properties of α - Al_2O_3 nanoparticles using the sol-gel method, Chem. Data Collect., 29 (2020) 100531. https://doi.org/10.1016/j.cdc.2020.100531

[27] C. Piconi ,G. Maccauro, Zirconia as a ceramic biomaterial, Biomaterials, 20 (1999) 1-25.

[28] J. Safaei-ghomi, S. Zahedi, M. Javid, M. A. Ghasemzadeh, MgO Nanoparticles : an Efficient , Green and Reusable Catalyst for the One- pot Syntheses of 2 , 6-Dicyanoanilines and 1 , 3-Diarylpropyl Malononitriles, J. Nanostructures, 5 (2015) 153–160. https://doi.org/10.7508/jns.2015.02.010

[29] C. W. Wong et al., Response Surface Methodology Optimization of Mono-dispersed MgO Nanoparticles Fabricated by Ultrasonic-Assisted Sol–Gel Method for Outstanding Antimicrobial and Antibiofilm Activities, J. Clust. Sci., 31 (2020) 367–389. https://doi.org/10.1007/s10876-019-01651-3